1. INTRODUCTION

We have developed and implemented a new high-order low-order (HOLO) algorithm for solving thermal radiative transfer (TRT) problems. This algorithm has several desirable properties that improve on current computational methods for solving TRT problems. In particular, our HOLO method utilizes an exponentially-convergent Monte Carlo (ECMC) algorithm to solve the associated radiation transport equation. The ECMC method significantly decreases the statistical noise associated with MC calculations to TRT problems. In addition, we use a nonlinear low-order (LO) system to efficiently resolve nonlinear dependencies in system, while preserving accuracy of the ECMC treatment of particle transport. The HOLO algorithm has been developed and implemented for a simplified model with one spatial dimension and frequency-integrated equations.

The LO equations are formed with finite-element (FE) based spatial moments and angular moments over each half-range. A linear-discontinuous representation is used to discretized the temperature field. The LO equations are similar to S_2 equations, but contain intensity-weighted angular averages that are estimated via the HO solver. The LO solver is fully implicit in time and efficiently resolves the non-linear temperature dependence at each time step. The HO transport problem is a fixed-source, pure absorber transport problem, with sources defined by the previous LO solve. This transport equation is solved with ECMC simulation to produce a globally accurate solution. This global solution is used to compute consistency terms, which require the HO and LO solutions to converge towards the same solution. The use of ECMC allows for the efficient reduction of statistical noise in the MC solution, reducing inaccuracies introduced through the LO consistency terms.

We have also investigated several extensions of this method. In particular, we have investigated higher time accuracy by including the time variable in the ECMC transport algorithm.

We compare results with an implicit Monte Carlo (IMC) code for one-dimensional, gray test problems and demonstrate the efficiency of ECMC over standard Monte Carlo in this HOLO algorithm.

In the remainder of this chapter, we provide a background on TRT problems, discuss previous and related work, and then

1.1 Thermal Radiative Transfer Background

Thermal radiative transfer (TRT) physics describe the time-dependent energy distributions of a photon radiation field and a high-temperature material. The material and radiation exchange energy through absorption and emission of photons by the material. Accurate modeling of TRT physics becomes relevant in the high-energy, high-density physics regime. Radiative transfer is the dominant form of heat transfer in very high-temperature systems, where the material temperature T is $O(10^6)$ K or higher. Typical computational applications of TRT include simulation of inertial confinement fusion and astrophysics phenomena.

The transport of photons through a material is characterized by particle position, direction, and frequency. The material energy distribution is described by the material internal energy as a function of position. The high-dimensional space results in a nonlinear transport problem that is difficult to solve. The internal energy e is related to the material temperature through an equation of state. In this work a perfect gas equation of state is used [?], which produces the relation $\rho c_v T = e$, where ρ is the material mass density and c_v is the specific heat. Thus, we will now discribe the equations in terms of temperature.

The governing equations for thermal radiative transfer problems are the radiation and material energy balance equations:

$$\frac{1}{c}\frac{\partial I\left(\mathbf{r},\mathbf{\Omega},\nu,t\right)}{\partial t} + \mathbf{\Omega}\cdot\nabla I\left(\mathbf{r},\mathbf{\Omega},\nu,t\right) \tag{1.1}$$

The equations are strongly coupled through the gray Planckian emission source $\sigma_a acT^4$, which is a nonlinear function of temperature, and the radiation absorption term $\sigma_a\phi$. In general, the material properties are a function of T. The temperature-dependent material properties and absorption and reemission physics lead to systems that require accurate modeling of photon transport through a mix of streaming and optically-thick, diffusive regions. Although in most physical applications material motion is present, it is not the focus of this research and will not be considered. The purpose of the proposed research is to demonstrate the ability of a new algorithm to provide highly-accurate and efficient solutions to Eq. (1.2) and Eq. (1.3).

1.1.1   Derivation of 1D Grey Model

The transport of photons through a material is governed by the Boltzmann linear transport equation [?, ?]. We have demonstrated our method by applying it to a simplified model. make an assumption of isotropic scattering to simplify the equations. The radiative

This research will focus on a simplified 1D slab-geometry and frequency-integrated (grey) TRT model. The governing equations for this simplified model are the radiation and material energy balance equations

$$\frac{1}{c}\frac{\partial I(x,\mu,t)}{\partial t} + \mu\frac{\partial I(x,\mu,t)}{\partial x} + \sigma_t I(x,\mu,t) = \frac{\sigma_s}{2}\phi(x,t) + \frac{1}{2}\sigma_a acT^4(x,t) \tag{1.2}$$

$$\rho c_v \frac{\partial T(x,t)}{\partial t} = \sigma_a\phi(x,t) - \sigma_a acT^4(x,t). \tag{1.3}$$

In the above equations the fundamental unknowns are the material temperature $T(x,t)$ and the angular intensity $I(x,\mu,t)$ of radiation, where x is the position, t is the time, μ is the x-direction cosine of the photon direction of travel, and a, c, ρ, and c_v are the radiation constant, speed of light, material mass density, and material specific heat; σ_a, σ_s, and σ_t are the absorption, scattering, and total cross sections (cm^{-1}), respectively. The scalar radiation intensity $\phi(x,t) = \int_{-1}^{1} I(x,\mu,t)\mathrm{d}\mu$ is related to the radiation energy density E (with typical units Jks cm^{-3} sh^{-1}) by the relation $E = \phi/c$.

1.1.2 The Monte Carlo method for Particle Transport

1.2 Previous Work

This sections describes related work on Monte Carlo solution to the TRT equations. The Monte Carlo (MC) method samples the underlying physics distributions to estimate the average behavior of a field of photon. This can provide a highly-accurate results, in particular for treatement of the angular and temporal variable in the transport equation. The temperature equation is almost always solved deterministically in such particle transport methods. Monte carlo solution to the transport equation can introduce larege statistical noise into the material temperature distribution, which is undesirable when coupling to other physics. To improve the efficiency of MC solutions, hybrid MC methods utilize a deterministic solution to accelerate the MC solution.

1.2.1 The Implicit Monte Carlo Method

Monte Carlo (MC) solution to the TRT equations is typically achieved by the implicit Monte Carlo (IMC) method [?]. This method partially linearizes Eq. (1.2) & Eq. (1.3) over a discrete time step, with material properties evaluated at the previous temperature. Linearization of the system produces a transport equation that contains

4

an approximate emission source and an effective scattering cross section representing absorption and reemission of photons over a time step. This transport equation is advanced over a time step via MC. The MC simulation tallies energy absorption over a discretized spatial mesh. The energy absorption in each mesh cell is used to directly estimate a new end of time step temperature in that cell. In optically thick regions, or for large time steps, the effective scattering dominates interactions. In these diffusive regions IMC becomes computationally expensive. Acceleration methods typically attempt to improve efficiency by allowing particles to take discrete steps through optically thick regions based on a discretized diffusion approximation [?, ?]. In IMC the approximate linearization of the emission source is not iterated on within a time step due to the large computational cost of the MC transport each time step; this imposes a limit on the time step size to produce physically accurate results [?].

The Monte Carlo (MC) method [?] is a standard computational method in the field of radiation transport. The implicit Monte Carlo (IMC) method [?] is the most common approach for applying the MC method to TRT problems. The IMC method partially linearizes Eq. (1.2) and Eq. (1.3) over a discrete time step and lags material properties to produce a linear transport equation, which can be solved with MC simulation. The linear transport equation contains an approximate emission source and effective scattering cross section that represent absorption and reemission of photons over a time step. The transport equation is solved with MC simulation to advance the distribution of radiation to the end of the time step and determine the energy absorbed by the material over the time step. The energy absorption by the material is tallied over a discrete spatial mesh, computed with cell-averaged quantities. The energy absorption in each mesh cell is used to directly estimate a new end of time step material temperature based on the linearized material energy balance equation. Integration of the time-variable is treated continuously over the

time step via MC sampling, but the linearized Planckian source in the transport equation is based on a time-discrete approximation.

The IMC method has some limitations. In optically thick regions, or for large time steps, the effective scattering dominates interactions. In these diffusive regions IMC becomes computationally expensive. Acceleration methods typically attempt to improve efficiency by allowing particles to take discrete steps through optically-thick regions based on a spatially-discretized diffusion approximation [?, ?]. Another issue occurs due to the approximate linearization of the system which can not be iteratively improved due to the high computational cost of the MC transport. For some problems, the linearization can yield non-physical results that violate the discrete maximum principle if the time step size is too large or the cell size is too small [?]. The violation of the maximum principle results in the material temperature being artificially higher than the boundary conditions and sources should physically allow. The violation is caused by the temperature in the emission source not being fully implicit in time due to the necessary linearization. The work in [?] uses less-expensive MC iterations to produce an implicit system which prevents this from happening, but has very slow iterative convergence in diffusive problems. In IMC, temperature-dependent material properties, in particular cross sections, are evaluated at the previous-time step temperature. These lagged cross sections can produce inaccurate solutions but do not cause stability issues.

In IMC the material and radiation energy fields are discretized spatially to solve for cell-averaged values. Inaccurate spatial representation of the emission source over a cell can result in energy propagating through the domain artificially fast, yielding non-physical results referred to as "teleportation error" [?]. The IMC method uses a fixup known as source tilting to mitigate this problem. Source tilting reconstructs a more accurate linear-discontinuous representation of the emission source within a

cell based on the cell-averaged material temperatures in adjacent cells. Recent work in IMC has incorporated a linear-discontinuous finite-element representation directly into the discretization of the material temperature equation [?].

For TRT simulations, inaccurate spatial representation of the emission source over a cell can result in energy propagating through the domain artificially fast, yielding non-physical results referred to as "teleportation error" [?]. The IMC method uses a fixup known as source tilting to mitigate this problem. Source tilting reconstructs a more accurate linear-discontinuous representation of the emission source within a cell based on the cell-averaged material temperatures in adjacent cells. This linear reconstruction is also necessary to preserve the asymptotic equilibrium diffusion limit (EDL), at least for a more general time step size and class of problems than for a piece-wise constant representation [?]. Preserving the equilibrium diffusion limit is an important aspect of a numerical method for TRT problems. In this limit, cells are optically thick and diffusive, and the material and radiation energy fields approach equilibrium. Spatial discretizations which do not preserve the EDL can produce inaccurate solutions, even though the mesh size should accurately capture the behavior of the solution [1].

1.2.2 Previous work on moment-based acceleration methods

An alternative application of MC to the TRT equations is moment-based hybrid MC methods. Recent work has focused on so-called high-order low-order (HOLO) methods [?, ?, ?, ?]. These methods involve fixed-point iterations between high-order (HO) MC solution of a transport equation and a deterministic LO system. The low-order (LO) operator is based on angular moments of the transport equation, formulated over a fixed spatial mesh. Physics operators that are time consuming for MC to resolve, e.g., absorption-reemission physics, are moved to the LO system. The

7

reduced angular dimensionality of the system and Newton methods allow for non-linearities in the LO equations to be fully resolved efficiently [**?**, **?**]. The high-order (HO) transport problem is defined by Eq. (1.2), with sources estimated from the previous LO solution. The high-order (HO) transport equation is solved via MC to produce a high-fidelity solution for the angular intensity. The MC estimate of the angular intensity is used to estimate consistency terms, present in the LO equations, that require the LO system to preserve the angular accuracy of the MC solution. These consistency terms are present in all spatial-regions of the problem, requiring statistical variance to be reduced sufficiently throughout the entire domain of the problem.

Another area of related research is the application of residual Monte Carlo. The goal of these methods is to solve an auxiliary transport equation for the error in some estimate of the intensity. The error is then added to the estimate of the solution, which can produce an overall solution for the intensity that has less statistical noise than solution of the original transport equation would produce. In [**?**], the MC simulation solves for the change in intensity from the previous time step. This has the potential to limit statistical noise significantly in regions where the solution is near equilibrium. The work in [**?**] used residual MC as a HO solver for 1D grey problems. The residual MC demonstrated impressive reduction in statistical variance. However, a piecewise constant representation was used for the space-angle representation of the intensity, which does not preserve the EDL and can be inaccurate in angularly complex regions of the problem. Similar to RMC, a difference formulation has been applied to another algorithm known as the symbolic IMC method (SIMC), for the case of 1D frequency-dependent problems [**?**]. SIMC forms a standard FE solution to the material energy balance equation, and uses symbolic weights in the MC transport to solve for expansion coefficents. The difference formulation modifies the transport

equation to solve for unknowns representing the deviation of the intensity from equilibrium with the material energy. The difference formulation was also applied to a linear-discontinuous FE spatial representation of the emission source, demonstrating accuracy in the EDL [?]. Both [?] and [?] produced minimal statistical noise in slowly varying problems where the behavior of the system is near equilibrium.

1.3 Overview of the HOLO Algorithm

The research proposed herein provides a new HOLO algorithm for radiative transfer. In this work, we propose an S_2-like LO operator [?] in conjunction with an exponentially-convergent MC (ECMC) method [?] for the HO solver. Our LO system and approach to enforcing consistency contrast greatly from the typical formulation in [?, ?, ?]. We have derived the LO operator directly from the transport equation, using a linear-discontinuous finite-element (LDFE) spatial discretization. Exponentially-convergent Monte Carlo (ECMC)[?, ?] provides an iterative algorithm that can efficiently reduce statistical noise to acceptable levels with significantly less particle histories than standard MC. In particular, ECMC is exceptionally efficient in time-dependent TRT problems because information about the intensity from the previous time step can be used as an accurate initial guess for the new end of time step intensity. However, implementation of ECMC is non-trivial, requiring a finite-element representation of the solution in all phase-space variables that are being sampled with MC. The method contains many of the desired qualities, such as preserving the equilibrium diffusion limit, preserving the maximum principle, and in particular, providing high-fidelity MC solution to the TRT equations in an efficient manner.

Sufficient MC histories must be performed to eliminate statistical noise in the consistency terms that can contaminate the LO solution. Exponentially-convergent

Monte Carlo (ECMC)[**?**, **?**] provides an algorithm that can efficiently reduce statistical noise to the same order as the HOLO iteration error with significantly less particle histories than standard MC. In particular, ECMC is exceptionally efficient in time-dependent TRT problems because information about the intensity from the previous time step can be used as an accurate initial guess for the new end of time step intensity. Additionally, no particle histories are required in regions where the radiation and material energy field are in equilibrium, similar to [**?**]. However, implementation of ECMC is non-trivial, requiring a finite-element representation of the solution in all phase-space variables that are being sampled with MC. The fundamental transport of particles is the same as standard Monte Carlo transport codes, but the source will now contain positive and negative weight particles.

1.3.1   Similarities to Residual Monte Carlo

Our ECMC solver contains similarities to the residual Monte Carlo (RMC) HO solver in [**?**], with some key differences. The RMC algorithm uses a particular, fixed estimate of the solution to significantly reduce the statistical noise in the simulation compared to a standard MC simulation. The guess for the solution is chosen to produce only sources on the faces of cells, reducing the dimension of the phase-space to be sampled [**?**]. The RMC algorithm uses a piecewise constant trial space representation for the intensity in x and μ. The primary difference between the methods is that ECMC iteratively estimates the solution, in batches, producing a known MC estimate of the error in that estimate. The ECMC algorithm projects the intensity onto a linear-discontinuous finite-element (LDFE) trial space, although the RMC algorithm could similarly be formulated with an LDFE representation. Adaptive mesh-refinement can be used in ECMC to produce highly accurate solutions with minimal statistical noise, as long as sufficient particle histories are performed.

The formulation of the residual in [?] use an estimate of the solution such that only face sources need to be sampled. This residual formulation can produce minimal statistical noise in slowly varying problems where the behavior of the system is near equilibrium. Our ECMC algorithm has similar statistical efficiency by choosing the previous time step intensity as the initial guess to the algorithm; however, a linear volumetric source must be sampled in addition to face sources. The ECMC algorithm will generally be more efficient in cases where the solution varies greatly over a time step or when very low statistical noise is desired. Generally, the minimum number of histories per batch to obtain convergence with the LDFE trial space is larger than a piece-wise constant representation because additional histories are needed to sufficiently estimate the first moment in x and μ of the intensity. It is noted that our formulation of the LO equations and consistency terms contrast greatly from the typical formulation in [?, ?, ?].

In this work, we demonstrate the utility of an S_2-like LO operator [?] in conjunction with an ECMC method [?] for the HO solver. The ECMC algorithm uses information about the intensity from the previous time step to reduce statistical noise to the same order as the HOLO iteration error with significantly less particle histories than standard MC simulations, with less computational cost than IMC per history. We have derived the LO operator directly from the transport equation, using a linear-discontinuous (LD) finite-element (FE) spatial discretization for the HO and LO solutions. Herein we describe the algorithm and present results for 1D, gray test problems.

1.4   Dissertation Layout

This document describes dissertation research over a new Monte Carlo algorithm for solution of thermal radiative transfer problems. Herein, a brief description of

thermal radiative transfer and the model problem are given, followed by a discussion of the standard Monte Carlo solution method and other related research. An overview of the methodology and results performed thus far are given in Sec. **??**. Then, the remaining topics for completing this dissertation research are discussed in Sec. **??**. Finally, Sec. **??** provides a specific outline of the remaining research to be investigated and computational results to be generated.

2.   RESIDUAL MONTE CARLO TREATMENT OF THE TIME VARIABLE

Another extension and improvement for the HOLO method described in Sec. **??** is the time discretization of the transport equation. We have incorporated the time variable into the ECMC method to improve efficiency over IMC, while still preserving the accuracy of MC integration. The main area of interest is in producing more accurate resolution of radiation wave-fronts in optically thin regions, where particles transport a long distance over a time step. In such regions, the MC integration of the time variable by IMC can produce greater accuracy than an implicit Euler discretization, which can produce artificially fast propagation of radiation in space. A potential application where this accuracy is important is stellar atmosphere calculations. It is noted that no adaptive refinement in time is performed, so maintaining exponential convergence may not be possible. However, we still expect the residual MC formulation of the ECMC method to show improvement in efficiency over standard MC.

In the remainder of this chapter, the inclusion of the time variable into the ECMC trial space is detailed, along with modifications to particle tracking and the ECMC algorithm. The process of sampling, tracking, and tallies particle histories in time is detailed in literature[**?**, **?**, **?**, **?**], but sufficient details are provided in this chapter. Finally, a new temporal closure for the LO equations is given, and results are compared to IMC for accuracy and efficiency.

2.1   Modifications to the HO equations

Inclusion of the time variable t in the trial space used by ECMC allows for no discretization of the transport operator $\mathbf{L}$. The transport operator, applied to the

continuous intensity I, becomes

$$\mathbf{L}I(x,\mu,t) = \frac{1}{c}\frac{\partial I}{\partial t} + \mu\frac{\partial I}{\partial x} + \sigma_t I \tag{2.1}$$

The emission source is still treated with an implicit Euler discretization, which is similar to the approximation made in IMC. The ECMC algorithm specified in Sec. **??** does not need to be modified. However, the residual source and trial-space representation are modified to include t. Each batch is still estimating the error in the current projection estimate $\tilde{I}(x,\mu,t)$, but the time variable must be included in the inversion of the $\mathbf{L}$ operator.

2.1.1 The Doubly-Discontinuous Trial Space in Time

It is necessary to define a new trial space that includes the time variable so that we can explicitly evaluate the residual. The time variable has a similar representation to the LDD trial space used for the spatial variable in Sec. **??**, but the solution is a constant value over the interior of the time step. This step, doubly-discontinuous (SDD) trial space is defined as

$$\tilde{I}(x,\mu,t) = \begin{cases} \tilde{I}^n(x,\mu) & t = t^n \\ \overline{I}(x,\mu) & t \in (t^n, t^{n+1}) \\ \tilde{I}^{n+1}(x,\mu) & t = t^{n+1} \end{cases} \tag{2.2}$$

where we have used $\overline{I}$ to denote the time-averaged LDFE *projection* in x and μ of the intensity over the interior of the time step; the beginning and end of time step projections are denoted $\tilde{I}^n$ and $\tilde{I}^{n+1}$, respectively. An illustration of t for the SDD trial space, over the n-th time step, is depicted in Fig. 2.1. There is a projection error in using the LDFE projection to represent the intensity between time steps. However,

with sufficient noise reduction and mesh resolution, this should be an acceptable error compared to the large statistical noise of standard MC.
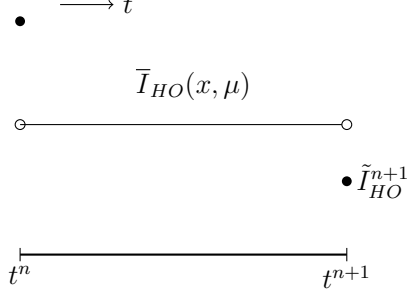

Figure 2.1: Step doubly-discontinuous representation of t for the HO solution.

The SDD trial space provides a projection for all the desired unknowns to exactly produce the moment equations, i.e., the time-averaged, end of time step, and previous time step intensities; temporally, these are the only unknowns that appear in equations that have been integrated over a time step to produce a balance statement. Another benefit of this trial space is it allows for infrastructure for computing the residual from the time-discrete case to be used directly. This trial space has one major drawback: only particle histories that reach t^{n+1} contribute to the estimation of $\tilde{\epsilon}^{n+1}$, and thus I^{n+1}. This is undesirable in optically thick problems.

REWRITE: Possibly move this to the future work section Alternatively, an LDFE representation could be used in the time variable. The linear representation would produce less noise because all particle tracks contribute to the slope, rather than just those that reach the end of the time step, although it would produce an approximate projection error for the end of time step intensity that is not produced with a discontinuity at the end of the time step. The linear representation in time would also

15

produce a more accurate reconstruction of the scattering source in time. However, a linear representation requires the sampling algorithm to be significantly modified because the L_1 integral for computing the residual magnitude is now significantly complicated by the tri-linear function. A possible way to sample this source is discussed in Appendix??? for completeness, but it has not been rigorously investigated.

2.1.2   Residual Source Definition and Sampling

The residual is defined as $r = q - \mathbf{L}\tilde{I}(x, \mu, t)$, where

$$q = \left(\sigma_a ac(T_{LO}^{n+1})^4(x) + \sigma_s \overline{\phi}_{LO}\right) \tag{2.3}$$

is a constant in time and provided by the LO solver. We have assumed a constant reconstruction for the scattering source in time. Evaluation of the residual with Eq. (2.2) for I produces a uniform source in time, as well as a δ-function source at the beginning and end of the time step. We write the residual source in terms of three components:

$$r(x, \mu, t) = \overline{r}(x, \mu) + r^n(x, \mu)\delta^+(t - t^n) + r^{n+1}(x, \mu)\delta^-(t - t^{n+1}), \quad t \in [t^n, t^{n+1}] \tag{2.4}$$

We will look at each component individually. The first residual term is a constant in time with representation

$$\overline{r}(x, \mu) = q - \mu\frac{\partial \overline{I}(x, \mu)}{\partial x} - \sigma_t \overline{I}(x, \mu) \tag{2.5}$$

Evaluation of the above function produces both face and volumetric sources, similar to in the discrete case. To sample x and μ from the face and volume distributions, the same rejection procedure can be used as for Eq. (**??**) and detailed in [**?**]. The

time variable can then be sampled uniformly over the time step, i.e., $t = t^n + \eta \Delta t$, where η is a uniform random variable with support $(0, 1)$.

The second source has definition

$$r^n(x, \mu) = -\frac{1}{c} \frac{\partial \overline{I}(x, \mu)}{\partial t}\bigg|_{t=t^n} = -\frac{1}{c}\left(\overline{I}(x, \mu) - \tilde{I}^n(x, \mu)\right) \tag{2.6}$$

This source is a LDFE space and angle volumetric source. The rejection sampling procedure is used to sample x and μ. All particles sampled from this source begin tracking with $t = t^n$.

The final source term is

$$r^{n+1}(x, \mu) = -\frac{1}{c} \frac{\partial \overline{I}(x, \mu)}{\partial t}\bigg|_{t=t^{n+1}} = -\frac{1}{c}\left(\tilde{I}^{n+1}(x, \mu) - \overline{I}(x, \mu)\right). \tag{2.7}$$

The source r^{n+1} can be treated using the same analytic treatment as the outflow face source in the LDD trial space, detailed in Sec. **??**; the source at the end of the time step is never sampled because its contribution to I^{n+1} can be analytically computed. To treat the sources this way, the solution for $\tilde{I}^{n+1}(x, \mu)$ is initialized to the value of $\overline{I}(x, \mu)$ before a batch of particles begins. Then, error particles that reach the end of the time step, referred to as "census" particles, contribute a standard score to the projection $\tilde{I}^{n+1}(x, \mu)$.

With these definitions, it is thus only necessary to sample from two sources. Using composite-rejection sampling [**?**], a discrete probability distribution is sampled to determine which source component to sample, followed by sampling of that component. The algorithm is

1. Sample uniform random number η

2. If $\eta < \|r^n\|_1 / (\|r^n\|_1 + \|r^{n+1}\|_1)$:

- Sample from r^n source using rejection sampling

- Sample t uniformly over (t^n, t^{n+1}).

3. Else:

- Sample from $\bar{r}$ source

All L_1 integrals can be analytically integrated using the same numerics as in the time-discrete case. The systematic sampling algorithm, as described in Sec. **??**, can be applied similarly. However, the choice of source is only make locally over that space-angle element. In that case, the element is chosen systematically, then the choice of r^n or $\bar{r}$ is sampled. REWRITE: Only discuss sampling of systematic case.

2.1.3 Importance Sampling on Interior of Time Step

As an attempt to reduce variance in the estimate of $\tilde{\epsilon}^{n+1}(x, \mu)$, we use important sampling in the time variable. Systematic sampling is still used for determining the cell of interest, and sampling as described above is used to determine which source is sampled, based on the appropriate probabilities described in the previous section. However, when the interior source $\bar{r}(x, \mu)$ is sampled, we use importance sampling for the conditional sampling of the uniform time step. The goal is to ensure that some histories reach the end of the time step. In order to do this, we sample from a modified PDF such that a fraction p_{end} of particles sampled from $\bar{r}(x, \mu)$ are born with $t \in (t^{end}, t^{n+1})$. We define $t^{end} = t^{n+1} - M/(c\sigma_t)$, where M is the desired number of MFP of travel the particle will undergo from the end of the time step (e.g., 2 or 3). The weights of particles sampled from this distribution must be modified to prevent source biasing.

The new PDF to be sampled from is

$$f^*(t) = \begin{cases} \dfrac{1 - p_{end}}{t^{end} - t^n} & 0 < t < t^{end} \\[2ex] \dfrac{p_{end}}{t^{n+1} - t^{end}} & t^{end} \le t < t^{n+1} \\[2ex] 0 & \text{elsewhere} \end{cases} \tag{2.8}$$

The original PDF is $f(t) = 1/\Delta t$, for $t \in (t^n, t^{n+1})$. Thus, using the standard procedure for importance sampling[?], the starting time t_{start} is sampled from $f^*(t)$, and then weights are multiplied by the factor $f(t_{\text{start}})/f^*(t_{\text{start}})$. This procedure is not perfect in that if a particle is moving from an optically thin to an optically thick region, it is not guaranteed to reach census. However, this case does not introduce bias.

2.1.4 Tracking and Tallying in Time

Because our LO equations will be integrated over the time step, we only need to perform MC tracking for $t \in [t^n, t^{n+1}]$. The initial time for the particle is sampled as described in the previous section. In inverting the **L** operator, particles are tracked until they reach the end of the time step. Path lengths are sampled or the weight is exponentially attenuated as before (e.g., Sec. **??**). As a particle travels from position x_o to x_f, with direction μ, the time is updated as

$$t^f = t^0 + \frac{|x_f - x_o|}{c\mu} \tag{2.9}$$

where c is the speed of light. For analog path-length sampling, if $t^f > t^{n+1}$ then t^f is adjusted to t^{n+1} and the path length is adjusted accordingly. For continuous weight deposition, particles are only tracked until they reach t^{n+1}. A proof that this process of tracking particles is a MC solution to an integral equation that is exactly inverse

19

to the **L** operator is detailed in [**?, ?**].

Tallies must be adjusted to account for the averaging over the time step, and to compute the intensity at the end of time step. To produced the time-averaged representation $\overline{I}(x, \mu)$, requires estimators for the average, x, and μ moments of the error, e.g.,

$$\overline{\epsilon}_{x,ij} = \frac{1}{\Delta t} \frac{6}{h_j} \int\limits_{t^n}^{t^{n+1}} \mathrm{d}t \int\limits_{x_{i-1/2}}^{x_{i+1/2}} \mathrm{d}x \int\limits_{\mu_{j-1/2}}^{\mu_{j+1/2}} \mathrm{d}\mu \ \left(\frac{x - x_j}{h_i}\right) \epsilon(x, \mu, t) \tag{2.10}$$

with a similar definition for the average and μ moments. The estimators are defined as

$$\hat{\overline{\epsilon}}_{x,ij} = \frac{1}{N_{hist}} \frac{6}{\Delta t h_i} \sum_{n=1}^{N_{hist}} \frac{s_n}{h_i h_j} w_j \left(x_c - x_i\right), \tag{2.11}$$

where the magnitude of the weights produce the L$_1$ integral over all phase space, i.e.,

$$\sum_{n=1}^{N} w_n = \|r(x, \mu, t)\|_1 \equiv \int\limits_{t^n}^{t^{n+1}} \mathrm{d}t \int\limits_{x_{i-1/2}}^{x_{i+1/2}} \mathrm{d}x \int\limits_{\mu_{j-1/2}}^{\mu_{j+1/2}} \mathrm{d}\mu \ |r(x, \mu, t)|. \tag{2.12}$$

Here, x_c is the center of the n-th path length, and s_n is the path length for the n-th path length in the $x - \mu$ cell.

Moments of $I^{n+1}(x, \mu)$ must be estimated to represent the end of time step intensity. For example, the x moment for the ij-th cell of the error at the end of time step is

$$\epsilon_{x,ij}^{n+1} = \frac{6}{h_i} \iint\limits_{\mathcal{D}_{ij}} \left(\frac{x - x_i}{h_i}\right) \epsilon(x, \mu, t^{n+1}) \mathrm{d}x \mathrm{d}\mu \tag{2.13}$$

The estimators for these moments are a generalization of the census tallies used in IMC [**?, ?**]. The tallies are based on the definition of the intensity as $I(x, \mu, t) = ch\nu N(x, \mu, t)$ given in Eq. (**??**), similar to collision estimators [**?, ?**]. The census

estimator for the x moment is

$$\hat{\epsilon}_{x,ij}^{n+1} = \frac{1}{N_{hist}} \frac{6}{h_j h_i} \sum_{n=1}^{N_{hist}} cw_j (x_c - x_i) \qquad (2.14)$$

Similar tallies are defined for the other space-angle moments. These tallies can be exceptionally noisy because only particles that reach the end of the time step contribute.

2.2 Closing the LO Equations in Time

The LO equations must be closed in time consistently with the HO equations. Previous work has enforced consistency in time by adding a local artificial source to the time-discretized LO equations in each cell [**?**]. This source was approximated based on the difference between the exact HO integral of the time derivative and the approximate representation in the LO equations. The advantage of this form is that the LO solver exclusively deals in time-averaged unknowns for the radiation terms in the equations. However, if the problem is strongly non-linear or the time-averaged and time-edge values differ greatly, this may become unstable.

We will alternatively use a parametric closure in the time variable, similar to the spatial closures discussed in the Sec. **??**. The time-integrated LO equations can be written exclusively in terms of time-averaged unknowns. This closure produces LO equations that have the same numerical difficulty to solve as the BE, fully-discrete LO equations, but have the potential to preserve the accuracy of the MC integration in time, upon non-linear convergence of the system. A closure relation is used to eliminate the end of time step moments present from the time derivative term. We will investigate different parametric forms of the closure for robustness. Once the time-averaged unknowns have been calculated, the time closures can be used to convert the time-averaged unknowns to end-of-time-step values.

REWRITE THIS SENTENCE One potential benefit of the time closure parameters is that $\overline{I}^{HO}$ will be most different from $I^{HO,n+1}$ in problems that are optically thin. In such problems, σ_a is small, leading to an optically thin problem. However, there may be difficulties in the MPV problems where the problems are tightly coupled and nonlinear, but can lead to a large change over a time step.

REWRITE: I think most of these paragraphs can be moved to intro

2.2.1   Derivation of Time-Averaged Moment Equations

The time-continuous radiation equations are integrated in space and angle the same as before. For example, the L and $+$ moment equation is

$$\frac{1}{c}\frac{\partial}{\partial t}\langle\phi\rangle_L^+ - 2\left(\mu_{i-1/2}I_{i-1/2}\right)^+ + \langle\mu I\rangle_{L,i}^+ + \langle\mu I\rangle_{R,i}^+ + \sigma_{t,i}h_i\langle\phi\rangle_{L,i}^+ - \frac{\sigma_{s,i}h_i}{2}\left(\langle\phi\rangle_{L,i}^+ + \langle\phi\rangle_{L,i}^-\right)$$
$$= \frac{h_i}{2}\langle\sigma_a acT^4\rangle_{L,i} \quad (2.15)$$

This equation is then integrated over the time step, and the emission source is assumed implicit. The same manipulations can be performed on the streaming term to form angular consistency terms, but the weighting fluxes are now time-averaged values. Thus, the angular consistency terms are computed with $\overline{I}(x,\mu)$. The equations with time-averaged consistency terms are

$$\frac{\langle\phi\rangle_{L,i}^{+,n+1} - \langle\phi\rangle_{L,i}^{+,n}}{c\Delta t} - 2\overline{\mu}_{i-1/2}^+\overline{\phi}_{i-1/2}^+ + \overline{\{\mu\}}_{L,i}^+\langle\overline{\phi}\rangle_{L,i}^+ + \overline{\{\mu\}}_{R,i}^+\langle\overline{\phi}\rangle_{R,i}^+ + \sigma_{t,i}^{n+1}h_i\langle\overline{\phi}\rangle_{L,i}^{n+1,+}$$
$$- \frac{\sigma_{s,i}h_i}{2}\left(\langle\overline{\phi}\rangle_{L,i}^+ + \langle\overline{\phi}\rangle_{L,i}^-\right) = \frac{h_i}{2}\langle\sigma_a^{n+1}acT^{n+1,4}\rangle_{L,i}, \quad (2.16)$$

These equations are exact at this point. The BE approximation is used for the temperature terms in the material energy equations, but the radiation energy deposition is a time-averaged valued. REWRITE: Maybe add material energy equation

2.2.2 Parametric Time Closure

The closure relations in time are different than the closure relations for the spatial variable because we do not have a slope in time. The following closure is a modified diamond relation:

$$I^{n+1} = 2\gamma\overline{I} - I^n \qquad (2.17)$$

where γ is the closure factor and $\overline{I}$ is the time-averaged intensity. A modified BE discretization can also be used:

$$I^{n+1} = \gamma\overline{I} \qquad (2.18)$$

The chosen closure relation must be used to eliminate the unknowns at t^{n+1} from each of the LO moment equations, with the values from the previous time step taken as a known quantity. Thus, it is necessary to have a closure relation for each moment and half range, producing four closure parameters per spatial cell. The closure relations for the L moment and the modified diamond relation are

$$\langle\phi\rangle_{L,i}^{\pm,n+1} = 2\gamma_{L,i}^{\pm}\langle\overline{\phi}\rangle_{L,i}^{\pm} - \langle\phi\rangle_{L,i}^{\pm,n} \qquad (2.19)$$

with equivalent definitions for the R moment. Substitution of the above equation into Eq. (2.16)

$$\frac{2}{c\Delta t}\left[\gamma_{L,i}^{+}\langle\phi\rangle_{L}^{+,n+1} - \langle\phi\rangle_{L}^{+,n}\right] - 2\overline{\mu}_{i-1/2}^{+}\overline{\phi}_{i-1/2}^{+} + \overline{\{\mu\}}_{L,i}^{+}\langle\overline{\phi}\rangle_{L,i}^{+} + \overline{\{\mu\}}_{R,i}^{+}\langle\overline{\phi}\rangle_{R,i}^{+} + \sigma_{t,i}^{n+1}h_i\langle\overline{\phi}\rangle_{L,i}^{n+1,+}$$
$$- \frac{\sigma_{s,i}h_i}{2}\left(\langle\overline{\phi}\rangle_{L,i}^{+} + \langle\overline{\phi}\rangle_{L,i}^{-}\right) = \frac{h_i}{2}\langle\sigma_a^{n+1}acT^{n+1,4}\rangle_{L,i}, \quad (2.20)$$

The other moment equations are analogously defined.

The value of $\gamma_{L,i}^{+}$, $\gamma_{R,i}^{+}$, $\gamma_{L,i}^{-}$, and $\gamma_{R,i}^{-}$ can be computed by substituting the trial-space representation of $I^{HO}(x,\mu,t)$ into Eq. (2.19) and its analogs.

2.3 Computational Results

We will test the HO time closure for several problems that characterize potential physics regime. Throughout this section, for the HOLO method, results that use the backward Euler discretization are indicated with HOLO-BE and the MC-based time closure are indicated with HOLO-TC, where applicable. For simplicity, all HOLO results have used the lumped-relation in the LO radiation moment equations to preserve positivity. We will compare sample statistics and accuracy against IMC simulations. The systematic sampling algorithms detailed in Sec. **??** and Sec. 2.1.2 were used for all HOLO results in this section. In the algorithm the average is set to the floor value and slopes to zero in such cells.

2.3.1 Near-Void Problem

For the first problem, the material properties are uniform throughout a 2.0 cm wide domain with $\rho c_v = 0.01374$ Jks cm^{-3} keV^{-1}, $\sigma_a = 10^{-6}$ cm^{-1}, and $\sigma_s = 0$ cm^{-1}. The material and radiation are initially in equilibrium at a temperature of 0.01 keV. An isotropic incident intensity with $T_r = 0.150$ keV is applied at $x = 0$ for $t > 0$; the incident intensity on the right boundary is 0.01 keV. The simulation end time is 0.003 sh. Because the problem is optically thin, no importance sampling on the interior of the time step is used. For this problem, we expect IMC to be accurate because the small opacity leads to the material energy equation being mostly uncoupled.
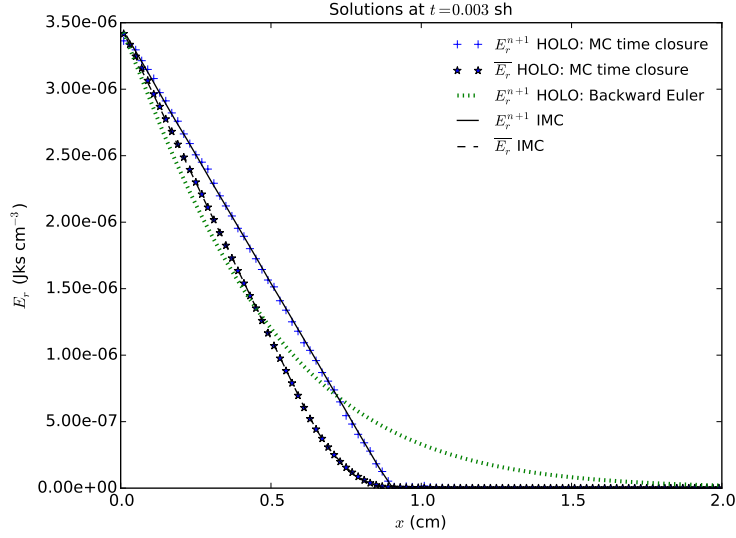
Figure 2.2: Comparison of radiation energy densities of IMC and HOLO method for the HO time closure and a BE discretization.

A comparison of the cell-averaged radiation energy densities E_r for IMC and the HOLO method with the diamond-like HO time closure are depicted in Fig. 2.2, both for the time-averaged solutions and end-of time step values, from the final time step. The end of time step value for the HOLO method with a BE discretization is also depicted. For the HOLO results, three ECMC batches were performed with a total of 3×10^6 histories per time step and the IMC results were generated with 12×10^6 histories per time step. The minimum number of histories for any sampled space-angle cell, N_{cut}??? in Eq. (**??**), is 20 for all HOLO simulations. The spatial meshs had 100 spatial cells and both HOLO results used 20 μ cells. The MC treatment of the time variable and the closure of the LO equations allow the LO results to correctly reconstruct the wave-front location of IMC, whereas the BE discretization artificially propagates energy. Although not plotted, the results were visually equivalent for either the diamond-like or implicit-like closures in this problem. This is because

25

the problem is nearly linear due to the small opacities, so the HO moments are reproduced accurately, independent of the chosen closure equation.

A comparison of similar results, but plotted as radiation temperatures, is plotted in Fig. **??**. By plotting proportional to the fourth-root of the radiation energy density, the noise at low magnitudes past the wave-front are more apparent in the 3 batches and $\Delta t = 0.001$ case. This noise is small relative to the scale of E_r, but it demonstrates a defficiency of the trial space. The cause is from the step representation over the time step leading to particles sampled near the wave-front with a time near t^n that travel into the equilibrium region. It is noted this is not a bias, but rather an undersampling; if sufficient histories were performed there would be negative particles that canceled out this error. This effect is significantly reduced when a smaller time step is taken, although it increases the projection error between time steps.

For the case of a single batch, there is less noise past the wavefront because the choice of $I^n(x, \mu)$ and an initial guess for $I^{n+1}(x, \mu)$ prevents most particles from traveling past what the physical transport should allow. The discrepancy betweeen the IMC and HOLO solution near the foot of the wave is a result of the spatial discrepancy between the LDFE HO projection and the lumped LD LO equations; this dispersion is not present in the HO solution. This discrepancy can also lead to some negativities in the LD representation of $\phi^{n+1}(x)$, which are set to the floor value for the next calculation.
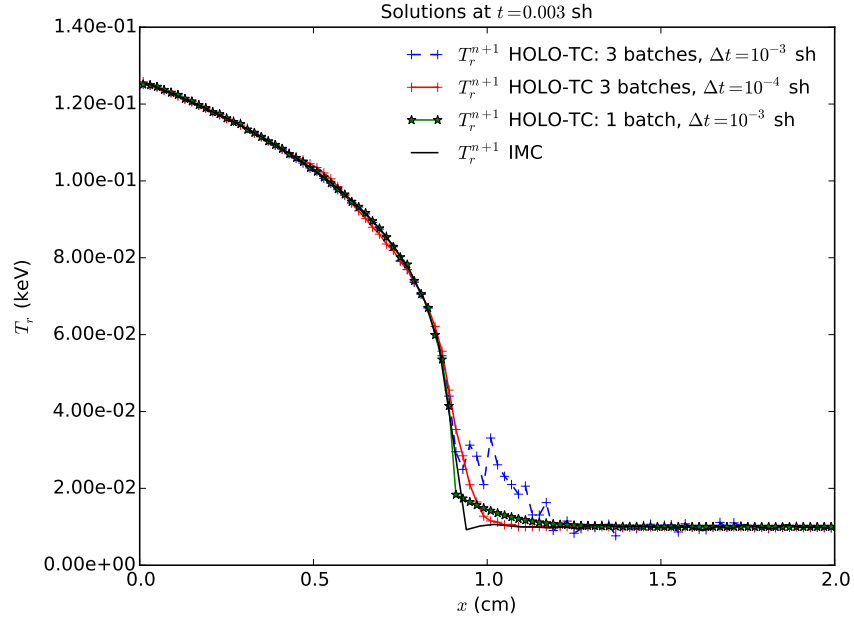
Figure 2.3: Comparison of radiation temperatures of IMC and the HOLO method for different time step sizes and numbers of batches, for the near-void problem.
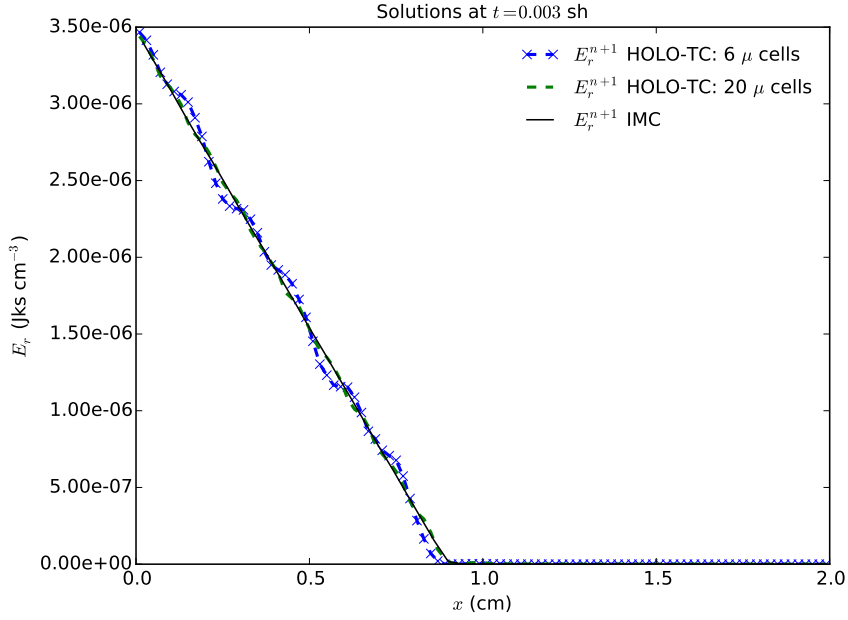
Figure 2.4: Comparison of radiation energy densities for the HOLO method with different numbers of μ cells. $\Delta t = 0.001$ sh, for near-void problem.

Figure. 2.4 compares radiation energy densities for various numbers of μ cells. At coarser mesh sizes, the imprinting of the mesh is visible in the location of the wave-front. This is a result of the projection onto the space-angle mesh between time steps. As the mesh is refined, the solution converges towards the IMC solution. Smaller time step sizes can increase the mesh imprinting because the projection onto the trial space happens more often. However, it is important to note that the mesh imprinting will be reduced as σ_a is increased and absorption-emission events smooth the angular intensity across each time step.

We have computed FOM statistics using Eq. (**??**) with 20 independent runs for each problem set up and parameters. The statistics are computed based on the time-averaged radiation energy densities. It is noted that the FOM results for each time step size are normalized to the IMC results within that table. The results

are compared for two different time step sizes in Tables 2.1 and 2.4. The different number of batches for the HOLO methods are indicated in parenthesis next to the method names. The results demonstrate that IMC can be more efficient than the ECMC method at longer time step sizes. This is a limiting case; because minimal absorptions are occuring in this problem, the IMC method is just advancing the initially sampled census particles between time steps, so there is negligible resampling of the phase space. Whereas, ECMC must resample the residual source and the step trial-space on the interior of the tiem step has a larger truncation error. At smaller time step sizes, the ECMC method, particularly for the single batch case, becomes more efficient than IMC.

Table 2.1: **Comparison of sample statistics for the time-averaged radiation energy densities, of the last time step, for the near-void problem and $\Delta t = 0.001$ sh. Simulation end time is t $= 0.003$ sh.**

hists./step	$\|s\|$			FOM		
	IMC	HOLO-TC (1)	HOLO-TC (3)	IMC	HOLO-TC(1)	HOLO-TC(3)
300,000	0.27%	0.27%	0.45%	1.00	0.96	0.35
3,000,000	0.09%	0.06%	0.15%	1.04	2.19	0.33

Table 2.2: **Comparison of sample statistics for the time-averaged radiation energy densities, of the last time step, for the near-void problem and $\Delta t = 10^{-4}$ sh. Simulation end time is t = 0.003 sh.**

	$\|s\|$			FOM		
hists./step	IMC	HOLO-TC (1)	HOLO-TC (3)	IMC	HOLO-TC(1)	HOLO-TC(3)
30,000	2.46%	0.44%	1.65%	1.00	31.07	2.22
300,000	0.80%	0.12%	0.37%	0.95	43.66	4.47

2.4 Optically Thin Problem

We modify the problem in the previous problem by increasing the absorption cross section to 0.2 cm^{-1}; all other problem parameters are the same. Radiation temperatures at the end of the last time step are compared for IMC, HOLO-TC, and HOLO-BE in Fig. 2.5. The HOLO-TC and HOLO-BE results were generated with 30 μ cells, and all spatial meshes used 200 cells. At smaller time step sizes, the effects of mesh imprinting are slightly apparent in the HOLO-TC results, leading to more dispersion near the wave-front. For $\Delta t = 0.005$ sh, there is good agreement between the HOLO-TC results and IMC. As in the previous problem, the HOLO-BE results do not accurately capture the wavefront location. IMC demonstrates substantial statistical noise in the equilibrium region.
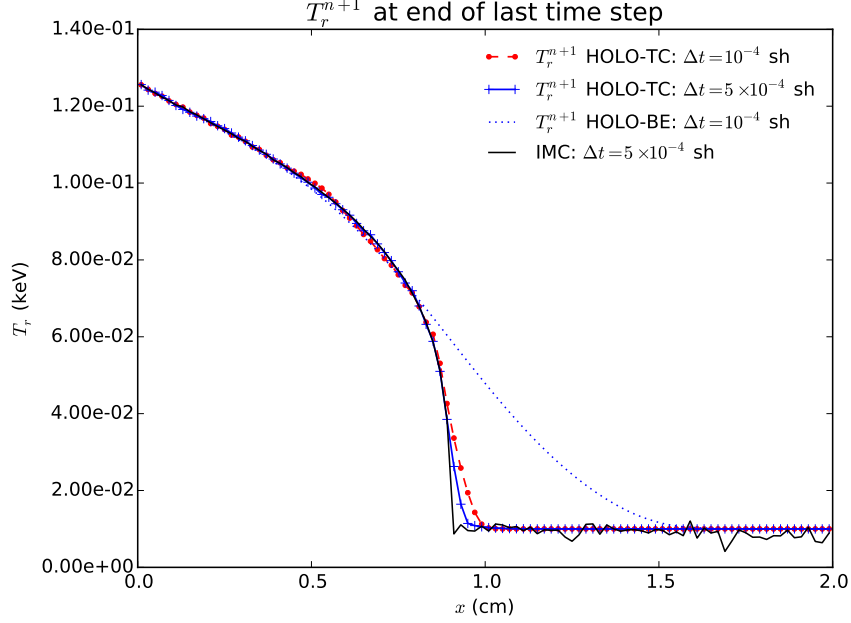
Figure 2.5: Comparison of radiation temperatures of IMC and the HOLO method for different time step sizes and numbers of batches, for optically thin problem. Time step size is $\Delta t = 0.002$ sh

Table. **??** compares computed FOM values for the census radiation energy densities, for the case of $\Delta t = 0.0005$ sh. HOLO results were generated for the case of 1 and 2 batches, with the same total number of histories per time step. At low particle counts for the larger time step size, the HOLO-TC method demonstrates substantial noise. This is due to the trial space representation of the census particles at the end of the time step being poorly estimated. For the 2 batch case, the estimate from the first batch leads to less error in the census estimate as the ECMC solves are simply solving for the deviation from the time-averaged quantity. The results for the case of 30,000 histories are plotted in Fig. **??** for the HO and LO solution. As demonstrated, there seems to have been some instabilities introduced into the LO equations through noise; sufficient sampling of the census must occur. At smaller

time-steps there is an increase in statistical efficiency, however there has been a loss in accuracy due to an increase in projection error. In general, this is a balance that much be considered.

The accuracy of the HOLO-ECMC method was compared to a reference solution from IMC. This problem is thin enough that we expect IMC to be accuracy with sufficient particle histories. The reference solution is the average of 20 IMC simulations of 20×10^6 histories, each with $\delta t = 10^{-4}$ sh. The estimated value of $\|s\|$ for the reference solution is 0.025%. The L_2 norm of the error in cell-averaged mean intensities is computed at the end of the last time step, was computed. The average over 20 simulations is then computed to provide the metric

$$\|e\|^l = \left(\frac{\sum\limits_{i=1}^{N_c} \left(\phi_i^{n+1,l} - \phi_i^{n+1,ref} \right)^2}{\sum\limits_{i=1}^{N_c} \left(\phi_i^{n+1,ref} \right)^2} \right)^{1/2}, \tag{2.21}$$

where $\phi_i^{n+1,l}$ is the cell-averaged scalar intensity at the end of the last time step from the l-th independent simulation. The sample mean of $\|e\|$ from 20 independent simulations provides a metric for the accuracy of a particular simulation:

$$\overline{\|e\|} = \frac{1}{20} \sum_{l=1}^{20} \|e\|^l \tag{2.22}$$

The accuracy results for

Table 2.3: **Comparison of sample statistics for the end of time step radiation energy densities, of the last time step, for the optically thin problem and $\Delta t = 5 \times 10^{-4}$ sh. Simulation end time is t = 0.003 sh.**

hists./step	$\|s\|$			FOM		
	IMC	HOLO-TC (1)	HOLO-TC (3)	IMC	HOLO-TC(1)	HOLO-TC(3)
30,000	3.01%	18.29%	5.38%	1.00	0.03	0.31
300,000	0.99%	0.81%	0.74%	0.93	1.38	1.65
1,000,000	0.50%	0.30%	0.37%	1.10	3.42	2.0

Table 2.4: **Comparison of sample statistics for the end of time step radiation energy densities, of the last time step, for the optically thin problem and $\Delta t = 1 \times 10^{-4}$ sh. Simulation end time is t = 0.003 sh.**

hists./step	$\|s\|$			FOM		
	IMC	HOLO-TC (1)	HOLO-TC (3)	IMC	HOLO-TC(1)	HOLO-TC(3)
30,000	3.00%	0.55%	1.28%	1.00	29.81	5.51
300,000	0.96%	0.11%	0.30%	0.98	71.82	9.88
1,000,000	0.49%	0.06%	0.17%	1.11	71.02	9.71

2.5   Two Material Problem

It is important to demonstrate that the time closures are stable in a mix of optically thick and optically thin regions, and that the ECMC method is still efficient in such problems. Simulations are performed for the two material problem defined in Sec. **??**. We use

REFERENCES

[1] J.E. Morel, T.A. Wareing, and K. Smith. Linear-Discontinuous Spatial Differencing Scheme for S_n Radiative Transfer Calculations. *Journal of Computational Physics*, 128:445–462, 1996.